Low-order modeling of the mutual synchronization between two turbulent thermoacoustic oscillators

Yu Guan
Department of Mechanical and Aerospace Engineering, The Hong Kong University of Science and Technology, Clear Water Bay, Hong Kong

Kihun Moon and Kyu Tae Kim*
Department of Aerospace Engineering, Korea Advanced Institute of Science and Technology, 291 Daehak-ro, Yuseong-gu, Daejeon 34141, Republic of Korea

Larry K. B. Li†
Department of Mechanical and Aerospace Engineering, The Hong Kong University of Science and Technology, Clear Water Bay, Hong Kong and Guangdong–Hong Kong–Macao Joint Laboratory for Data-Driven Fluid Mechanics and Engineering Applications, The Hong Kong University of Science and Technology, Clear Water Bay, Hong Kong

(Received 2 March 2021; revised 14 June 2021; accepted 2 August 2021; published 23 August 2021)

We use a low-order oscillator model to investigate the mutual synchronization of a thermoacoustic system consisting of two turbulent lean-premixed combustors coupled via a cross-talk tube. The model consists of two Van der Pol (VDP) oscillators coupled via dissipative and time-delay terms. We show that, despite its simplicity, the model can reproduce many of the synchronization phenomena observed experimentally, such as amplitude death, desynchronization (quasiperiodicity), synchronization (phase locking), and nonlinear energy pumping from a limit-cycle mode to a damped mode. This study shows that the mutual synchronization dynamics of a turbulent thermoacoustic system can be reproduced with just a simple coupled VDP model. This suggests that such a model could be used to identify new strategies for quenching limit-cycle oscillations in turbulent thermoacoustic systems, such as gas turbines and rocket engines.

DOI: 10.1103/PhysRevE.104.024216

I. INTRODUCTION

In many combustion systems, thermoacoustic instability can arise from the positive feedback between unsteady heat release and sound [1,2]. For example, when a flame interacts with the acoustic modes of a combustor, its heat release rate (HRR) can, under certain conditions, oscillate in phase with the pressure field, causing thermal energy to be transferred to the acoustic modes via the Rayleigh mechanism [3]. The pressure amplitude thus grows, but eventually saturates owing to the nonlinear HRR response of the flame [4], resulting in self-excited flow oscillations at the natural acoustic frequencies of the system [5]. If severe, such thermoacoustic oscillations can increase vibration and thermal stresses, degrading the reliability and efficiency of the overall combustion system [3].

The prediction and control of thermoacoustic oscillations have been the focus of many studies [6–10]. Traditionally, most studies have relied on the use of single combustors because this simplifies the geometry and analysis, while preserving the fundamental physics of the thermoacoustic feedback mechanisms. However, many practical combustion devices, such as gas turbines used for electricity generation, contain multiple combustors coupled to one another [11]. The thermoacoustics of such multicombustor devices cannot be fully understood by considering just a single isolated combustor, because of the possibility of bidirectional coupling between adjacent combustors [9,12]. Recognizing this, researchers have already begun to investigate the thermoacoustics of coupled combustors [13–15], but only a few have done so using synchronization theory. Synchronization theory provides an ideal framework for investigating thermoacoustic instability in multicombustor systems because (i) each combustor can be intuitively treated as an individual self-excited oscillator undergoing limit-cycle motion, and (ii) the bidirectional interactions between adjacent combustors can be modeled by introducing coupling terms between two identical or nonidentical self-excited oscillators [16–18]. This approach has led to the discovery of various synchronization phenomena, many of which have practical applications. For example, when two or more self-excited oscillators are coupled appropriately, each oscillator can become stabilized to a fixed point, causing the overall coupled system to stop oscillating altogether, i.e. to become quenched. This phenomenon, known as amplitude death (AD) [19], has been observed in systems as diverse as solid-state lasers and chemical reactors [20,21]. In thermoacoustic systems, AD could be used to suppress destructive flow oscillations arising from

*kt_kim@kaist.ac.kr
†larryli@ust.hk

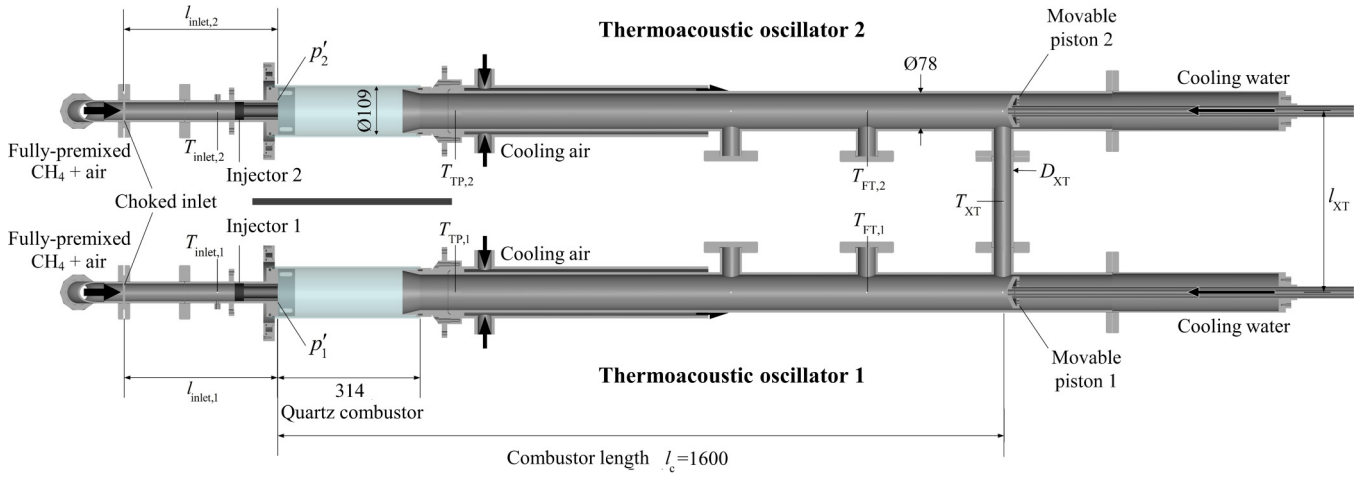

FIG. 1. Experimental setup consisting of two thermoacoustic oscillators coupled via a cross-talk tube whose diameter ($D_{XT} = 9.6$, 19.2, and 38.4 mm) and length ($l_{XT} = 320$, 400, and 480 mm) are independently adjustable. Each oscillator consists of a lean-premixed CH_4-air flame stabilized in the turbulent swirling flow (Re $\approx 4.4 \times 10^4$) of a cylindrical combustor whose length is fixed at $l_c = 1600$ mm. All dimensions shown are in millimeters. Further details can be found in Refs. [34,35].

the feedback between unsteady HRR and sound. Indeed, AD has already been experimentally observed in laminar thermoacoustic systems powered by porous stacks [22,23], electrically heated meshes [24], and Bunsen flames [25]. In general, various types of coupling can cause AD [26–30], but the two most common are dissipative and time-delay coupling. Low-order modeling has shown that when only dissipative coupling is present, AD can occur only when the frequency detuning is sufficiently large [31,32]. By contrast, when only time-delay coupling is present, AD can occur even for zero frequency detuning (i.e., identical oscillators), so long as the coupling parameters (strength and time delay) have appropriate finite values [26,32]. Crucially, the simultaneous presence of both dissipative and time-delay coupling has been shown to enlarge the region of parameter space in which AD occurs [22,32]. Other phenomena that have been observed in coupled thermoacoustic oscillators include in-phase and antiphase synchronization, phase-flip bifurcations, and partial amplitude death (PAD) [24]. PAD differs from AD in that only some of the coupled self-excited oscillators are quenched, while the others continue to oscillate [28,33].

The above observations were made in laminar systems, but practical combustors are almost always turbulent [3]. To better understand the thermoacoustics of such systems, we recently performed experiments on two turbulent lean-premixed combustors coupled via a cross-talk tube [34,35]. By analyzing the data in a synchronization framework, we were able to identify various phenomena, such as AD, phase locking (PL), and in-phase and antiphase synchronization [34,35]. However, although those experiments provided useful insight into the interactions between limit-cycle oscillations in a turbulent thermoacoustic system, they still fell short of offering a viable means of prediction and control. In the present study, we aim to address this issue by demonstrating that the mutual synchronization dynamics of two turbulent thermoacoustic oscillators can be reproduced with just a simple low-order model.

II. EXPERIMENTAL SETUP AND LOW-ORDER MODEL

Before introducing the low-order model, we first review the experiments [34,35] against which the modeling results will be compared. The experimental setup is based around two coupled thermoacoustic oscillators (Fig. 1). Each oscillator consists of a lean-premixed CH_4-air flame stabilized in the turbulent swirling flow of a cylindrical combustor whose length is fixed at $l_c = 1600$ mm. Also fixed are the bulk reactant velocity ($\overline{u_1} = \overline{u_2} = 40$ m/s) and the inlet temperature ($T_{\text{inlet},1} = T_{\text{inlet},2} = 200\,^{\circ}\text{C}$), resulting in an inlet Reynolds number of 4.4×10^4. We adjust the CH_4 and air flow rates independently using four thermal mass flow controllers (Teledyne Instruments HFM-D-301 for CH_4, and Sierra Instruments FlatTrak 780S for air). Upstream of each combustor is an inlet section whose length (l_{inlet}) is adjustable. Also adjustable is the equivalence ratio (ϕ) of the flame in each combustor. Depending on l_{inlet} and ϕ, each isolated thermoacoustic oscillator can occupy one of two states: (i) a steady state associated with a fixed point, and (ii) a self-excited oscillatory state associated with a limit-cycle attractor [34,35]. At the operating conditions of this study, transitions from the former state to the latter state usually occur via a supercritical Hopf bifurcation as either l_{inlet} or ϕ increases [34,35]. After the Hopf point, the amplitude and frequency of the limit-cycle oscillations depend on both l_{inlet} and ϕ [34,35]. We measure the pressure fluctuations in both combustors (p_1', p_2') using piezoelectric transducers (PCB 112A22) mounted at the injector plane (Fig. 1). We digitize the analog pressure signals from both combustors at 12 kHz for 4 s on a data logger (TEAC model LX-110).

To explore mutual synchronization, we couple the two thermoacoustic oscillators (combustors) to each other using a cross-talk tube whose diameter ($D_{XT} = 9.6$, 19.2, and 38.4 mm) and length ($l_{XT} = 320$, 400, and 480 mm) can be independently adjusted (Fig. 1). Increasing D_{XT} increases the cross-sectional area of the tube, increasing its acoustic admittance; this allows more acoustic energy to pass through the tube, increasing the coupling strength [24]. Increasing

l_{XT} increases the time required for information to travel between the two oscillators; this delay time can be quantified as l_{XT}/c, where c is the speed of sound [24]. We nondimensionalize both of these geometric coupling parameters as per Ref. [35]: $\epsilon \equiv D_{XT}/D_{XT,0}$, where $D_{XT,0} = 38.4$ mm is the baseline, and $\eta \equiv l_{XT}/l_c$, where l_c is the combustor length (fixed at 1600 mm, as noted earlier). Further details on the experimental setup can be found in Refs. [34,35].

We model the mutual synchronization between the two thermoacoustic oscillators using two Van der Pol (VDP) oscillators coupled via dissipative and time-delay terms:

$$\begin{aligned}\ddot{x}_1 - \left(\beta_1 - x_1^2\right)\dot{x}_1 + \omega_{n,1}^2 x_1 &= k_d(\dot{x}_2 - \dot{x}_1) \\ &\quad + k_\tau[\dot{x}_2(t-\tau) - \dot{x}_1], \\ \ddot{x}_2 - \left(\beta_2 - x_2^2\right)\dot{x}_2 + \omega_{n,2}^2 x_2 &= k_d(\dot{x}_1 - \dot{x}_2) \\ &\quad + k_\tau[\dot{x}_1(t-\tau) - \dot{x}_2], \quad (1)\end{aligned}$$

where the two oscillators are specified by subscripts 1 and 2, x_1 and x_2 are the dynamical variables ($\tilde{x}' \equiv x'/x'_{max}$), $\omega_{n,1}$ and $\omega_{n,2}$ are the natural angular frequencies in the linear limit, k_d is the dissipative coupling strength, k_τ is the time-delay coupling strength, τ is the time delay itself, and β_1 and β_2 are the excitation and damping parameters that control whether the solution converges to a fixed point ($\beta < 0$) or to a limit cycle ($\beta > 0$).

We calibrate the model [Eq. (1)] using the experimental data from Refs. [34,35]. To facilitate this, we normalize the pressure amplitude by the maximum pressure amplitude observed among all the decoupled thermoacoustic oscillators: $\tilde{p}' \equiv p'/p'_{max}$. Moreover, we normalize the frequency by the lowest limit-cycle frequency observed among all the decoupled thermoacoustic oscillators: $\tilde{f} \equiv f/f_{n,min}$. We then adjust β_1 and β_2 independently such that the ratio of the limit-cycle amplitudes between the two decoupled VDP oscillators matches that between the two decoupled thermoacoustic oscillators. Similarly, we adjust $\omega_{n,1}$ and $\omega_{n,2}$ independently such that the ratio of the limit-cycle frequencies is also matched. Here we are careful to account for the slight shift in the limit-cycle frequency as the oscillation amplitude increases [36–39]. Through this four-parameter calibration procedure, we achieve deviations in the amplitude ratio of less than 2.5% and in the frequency ratio of less than 0.1%. We believe that these deviation values are acceptable because our aim is to qualitatively reproduce the synchronization states observed experimentally, rather than to quantitatively reproduce the detailed flow features. The latter task is best left for high-fidelity numerical techniques such as large-eddy simulations, which are more computationally expensive than the low-order modeling approach taken in this study.

If a thermoacoustic oscillator is at a fixed point (rather than at a limit cycle), we calibrate its corresponding VDP oscillator using a heuristic approach. For example, we recall from the experiments of Jegal *et al.* [34] that the natural frequency of the thermoacoustic oscillator increases with ϕ. We therefore let ω_n increase with β. Moreover, we ensure that β is negative but increases to zero as the system approaches the supercritical Hopf point [40–42].

As for calibrating the coupling parameters (k_d, k_τ, and τ), we recall that the two thermoacoustic oscillators in our experiments are coupled via a single cross-talk tube, which implies that both dissipative and time-delay coupling occur through the same physical connection. On this basis, we let $k_d = k_\tau$, whose value we adjust in response to changes in ϵ in the experiments. Similarly, we adjust τ in response to changes in η. When adjusting k_d, k_τ and τ, we prioritize qualitatively reproducing the synchronization states observed experimentally [34,35], rather than quantitatively reproducing metrics such as the amplitude and frequency ratios. We numerically solve the coupled VDP model [Eq. (1)] using a fourth-order Runge–Kutta scheme. Next, we present a comparison of the experimental and numerical results.

III. RESULTS AND DISCUSSION

A. Symmetric inlet length: $l_{inlet,1} = l_{inlet,2}$

First we consider experiments in which the two thermoacoustic oscillators have the same inlet length ($l_{inlet,1} = l_{inlet,2} = 340$ mm) but a range of symmetric and asymmetric equivalence-ratio combinations ($\phi = 0.61$, 0.65, 0.69, and 0.73), with and without coupling [34,35]. These specific values of ϕ are used because they give rise to both fixed-point and limit-cycle attractors in the decoupled oscillators. Spectral data are shown in Fig. 2, where we label the different operating and coupling conditions as follows. For the decoupled oscillators (dark yellow borders), the uppercase "E" in front denotes experimental data (simulation data are denoted by "S"), the number after it specifies the particular oscillator (1 or 2), and the lowercase letter at the end specifies the value of ϕ as per (a, b, c, d) = (0.61, 0.65, 0.69, 0.73). For the coupled oscillators (light yellow borders), we combine the labels from two separate oscillators; for example, E1c-2b denotes the experimental case where oscillator 1c ($\phi = 0.69$) is coupled to oscillator 2b ($\phi = 0.65$).

On examining the decoupled thermoacoustic oscillators (Fig. 2: dark yellow borders), we find that each of them oscillates in a self-excited limit cycle when ϕ is low (Fig. 2: E1a, E2a, E1b, E2b), but that they transition to a fixed point when ϕ is high (Fig. 2: E1c, E2c, E1d, E2d). We find that these transitions occur in both thermoacoustic oscillators because, although decoupled, they have the same combustor geometry and are at the same operating conditions. Nevertheless, we also find noticeable differences in the spectral amplitude of the limit-cycle mode between any two nominally identical oscillators (Fig. 2: E1a vs. E2a; E1b vs. E2b). We attribute these differences to subtle variations in the operating conditions (e.g., ϕ and the reactant temperature and velocity), as well as to noise induced by turbulence in the reactive flow field.

On examining the coupled thermoacoustic oscillators (Fig. 2: light yellow borders), we find a variety of mutual synchronization phenomena. For example, quasiperiodicity (QP) arises from two incommensurate modes (Fig. 2: E1b–E2a, E1c–E2b). To demonstrate this, we show in Fig. 3(a1–c1) the phase portrait, Poincaré map, and slope of the correlation sum for a representative QP case (Fig. 2: E1b–E2a). Here we reconstruct the phase space using the embedding theorem of Takens [43], with a time delay of τ and an embedding dimension of d. We compute the correlation dimension ($\overline{D_c}$) using

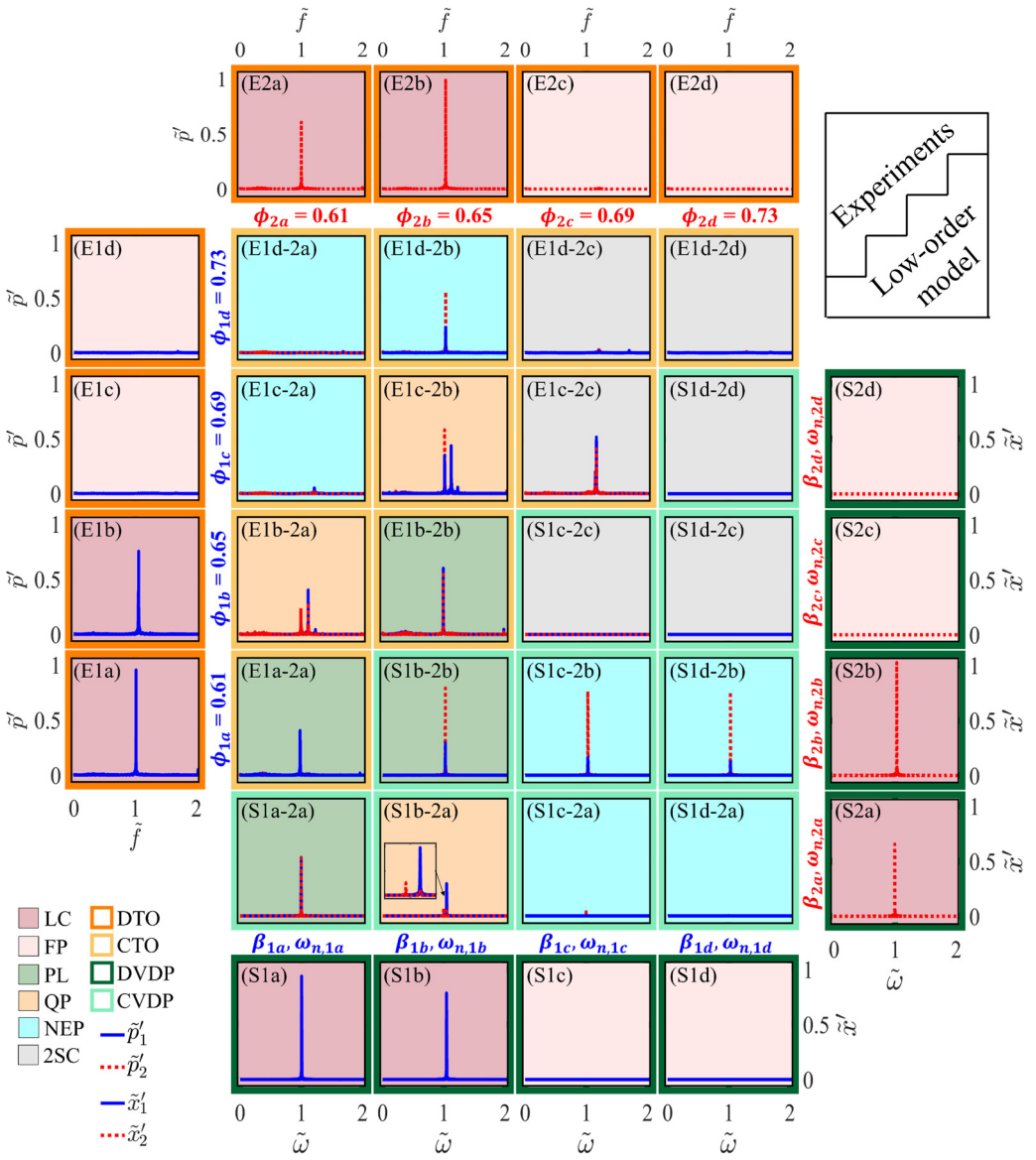

FIG. 2. Spectral comparison between thermoacoustic experiments (yellow borders) [34,35] and VDP simulations (green borders) under symmetric inlet-length conditions ($l_{\text{inlet},1} = l_{\text{inlet},2} = 340$ mm). The decoupled thermoacoustic oscillators (DTO: no cross-talk tube) and decoupled VDP oscillators (DVDP: $k_d = k_\tau = 0$) are denoted by dark yellow and dark green borders, respectively. The coupled thermoacoustic oscillators (CTO: $\epsilon = 1.0$, $\eta = 0.25$) and coupled VDP oscillators (CVDP: $k_d = k_\tau = 0.011$, $\tau = 1.6$) are denoted by light yellow and light green borders, respectively. Experimental calibration of the VDP model gives $(\beta_{1a}, \beta_{1b}, \beta_{1c}, \beta_{1d}) = (0.04, 0.03, -0.01, -0.02)$, $(\beta_{2a}, \beta_{2b}, \beta_{2c}, \beta_{2d}) = (0.02, 0.05, -0.01, -0.02)$, $(\omega_{n,1a}, \omega_{n,1b}, \omega_{n,1c}, \omega_{n,1d}) = (1.01, 1.05, 1.06, 1.07)$, and $(\omega_{n,2a}, \omega_{n,2b}, \omega_{n,2c}, \omega_{n,2d}) = (1.00, 1.03, 1.06, 1.07)$. Legend: LC = limit cycle; FP = fixed point; PL = phase locking; QP = quasiperiodicity; NEP = nonlinear energy pumping; 2SC = two steady oscillators coupled together.

the method of Grassberger and Procaccia [44]; this involves plotting the slope of the correlation sum (D_c) as a function of the hypersphere radius ($R/R_{\max}$) for different values of d, and then determining the value to which that slope converges over a finite range of $R/R_{\max}$. We find a noisy toroidal structure in the phase portrait [Fig. 3(a1)], which appears as a pair of fuzzy rings in the Poincaré map [Fig. 3(b1)]. This indicates that the phase trajectory spirals nonrepeatedly on an ergodic two-dimensional torus attractor ($\mathbb{T}^2$), a signature feature of QP arising from two incommensurate modes [45]. The correlation dimension of an ideal $\mathbb{T}^2$ torus attractor is $\overline{D_c} = 2$ [45]. However, we find a slightly higher value in our data [Fig. 3(c1): $\overline{D_c} \approx 2.5$] owing to the presence of turbulence-induced noise. Similar deviations of $\overline{D_c}$ have been observed in other turbulent thermoacoustic systems [46,47].

When one of the two thermoacoustic modes strengthens, their frequencies approach each other. Eventually, the two modes merge into one at a common global frequency, resulting in PL (Fig. 2: E1a–E2a, E1b–E2b). To demonstrate this, we show in Figs. 3(d1)–3(f1) the phase portrait, Poincaré map, and instantaneous phase difference between the two pressure signals ($\psi_{1,2}$) for a representative PL case (Fig. 2: E1a–E2a). Here we reconstruct the phase space as before, but compute $\psi_{1,2}$ with the Hilbert transform [48,49]. We find a noisy closed

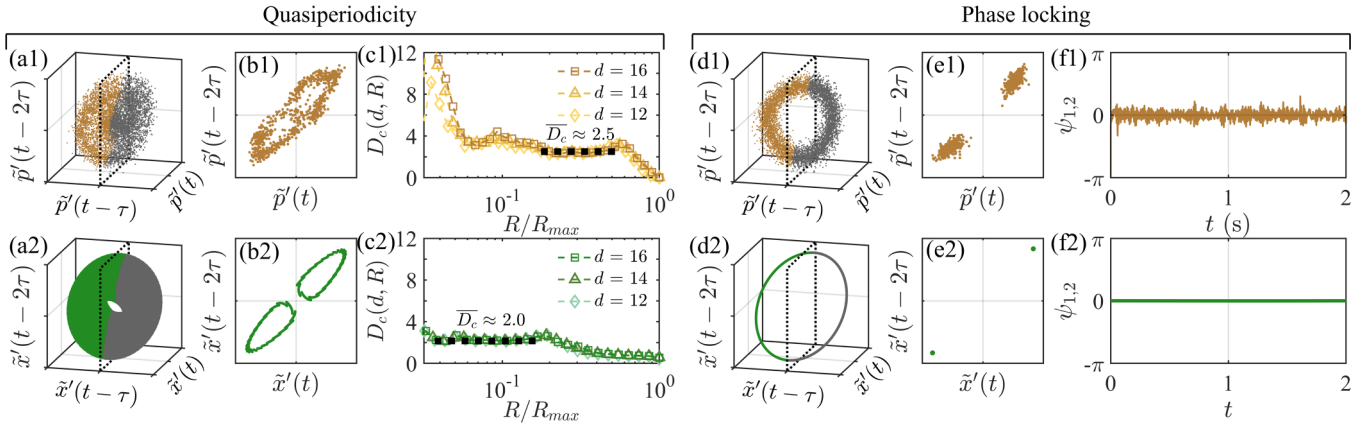

FIG. 3. (a1) Phase portrait, (b1) Poincaré map, and (c1) slope of the correlation sum for a QP state from the thermoacoustic experiments of Figs. 2(E1b)–2(E2a); analogous data from the VDP simulations of Fig. 2(S1b)–2(S2a) are shown immediately below in subfigures (a2–c2). Also shown are the (d1) phase portrait, (e1) Poincaré map, and (f1) instantaneous phase difference for a PL state from the thermoacoustic experiments of Figs. 2(E1a)–2(E2a); analogous data from the VDP simulations of Figs. 2(S1a)–2(S2a) are shown immediately below in subfigures (d2–f2).

orbit in the phase portrait [Fig. 3(d1)], which appears as two clusters of intercepts in the Poincaré map [Fig. 3(e1)]. Meanwhile, we find that the time-averaged slope of $\psi_{1,2}$ is zero [Fig. 3(f1)], indicating that the two thermoacoustic oscillators are evolving at the same time-averaged frequency [20,21]. There are, nevertheless, minor fluctuations in $\psi_{1,2}$ about its time-averaged value. These $\psi_{1,2}$ fluctuations appear to be stochastic, so we attribute them to turbulence-induced noise, rather than to phase trapping [50–52]. These observations confirm that the two thermoacoustic oscillators—which, when decoupled, are individually self-excited in limit cycles—are now coupled in such a way as to be undergoing PL [45].

There are three other synchronization phenomena of interest. First, under certain conditions (e.g., Fig. 2: E1c–E2b), coupling a steady oscillator (Fig. 2: E1c) to a limit-cycle oscillator (Fig. 2: E2b) can trigger a nonlinearly unstable mode whose frequency is controlled by the former oscillator but whose presence is felt in both oscillators. Such triggering is caused by the introduction of sufficiently strong disturbances to the initially steady oscillator (Fig. 2: E1c); here, such disturbances arise via coupling with the limit-cycle oscillator (Fig. 2: E2b). A similar triggering of nonlinearly unstable modes has been observed before in laminar and turbulent combustors [53,54]. After being triggered, the thermoacoustic mode in the initially steady oscillator (Fig. 2: E1c) interacts with that in the limit-cycle oscillator (Fig. 2: E2b). These two modes have incommensurate frequencies, producing ergodic $\mathbb{T}^2$ dynamics in the overall system.

Second, coupling two initially steady oscillators together can produce synchronized limit-cycle motion in both oscillators (Fig. 2: E1c–E2c). This is believed to be due to the destabilizing effects of the cross-talk tube; an explanation of this phenomenon can be found in Ref. [55].

Third, the amplitude of a limit-cycle oscillator can be partially (Fig. 2: E1d–E2b) or completely (Fig. 2: E1c–E2a, E1d–E2a) suppressed by coupling it to an initially steady oscillator. Such suppression is caused by a unidirectional irreversible transfer of energy from the limit-cycle oscillator to the initially steady oscillator. The latter element acts as an energy sink by localizing the incident energy and dissipating it via damping [56]. If the incident energy is low or if the dissipation is strong, the initially steady oscillator (energy sink) can remain steady, leaving the overall coupled system in a quiescent state (Fig. 2: E1c–E2a, E1d–E2a). In nonlinear dynamics, this is known as nonlinear energy pumping (NEP) [57,58] and is often associated with resonance captures [59]. NEP has been used to passively suppress self-excited oscillations in various systems, ranging from aeroelastic wings [60] to building structures [61]. However, to the best of our knowledge, this is the first experimental observation of NEP for passive suppression of self-excited instabilities in coupled thermoacoustic oscillators.

As for the VDP model [Eq. (1)], we find that it can reproduce many of the phenomena observed in the thermoacoustic system. In the QP case (Fig. 2: S1b–S2a → E1b–E2a), we find that the phase portrait and Poincaré map from the simulations [Figs. 3(a2) and 3(b2)] resemble those from the experiments [Figs. 3(a1) and 3(b1)]: the phase trajectory follows a nonrepeating path around an ergodic $\mathbb{T}^2$ torus attractor. However, the simulations produce a more defined attractor structure than the experiments, as evidenced by a cleaner pair of rings in the Poincaré map [Fig. 3(b2)]. We attribute this to the simulations being less noisy than the (turbulent) experiments. In turn, this lower level of noise enables the correlation dimension to take on the exact value expected for QP arising from two incommensurate modes [Fig. 3(c2): $\overline{D_c} = 2.0$].

In the PL cases (Fig. 2: S1a–S2a → E1a–E2a; S1b–S2b → E1b–E2b), we find that the simulations [Figs. 3(d2) and 3(e2)] produce a periodic attractor similar to that seen in the experiments [Figs. 3(d1) and 3(e1)]. As mentioned earlier, the simulations contain less noise than the experiments, causing $\psi_{1,2}$ to remain almost perfectly constant in time [Fig. 3(f2)], with none of the minor stochastic fluctuations seen in the experiments [Fig. 3(f1)]. Put together, these observations confirm that the limit-cycle oscillations of the two VDP oscillators are in a PL state.

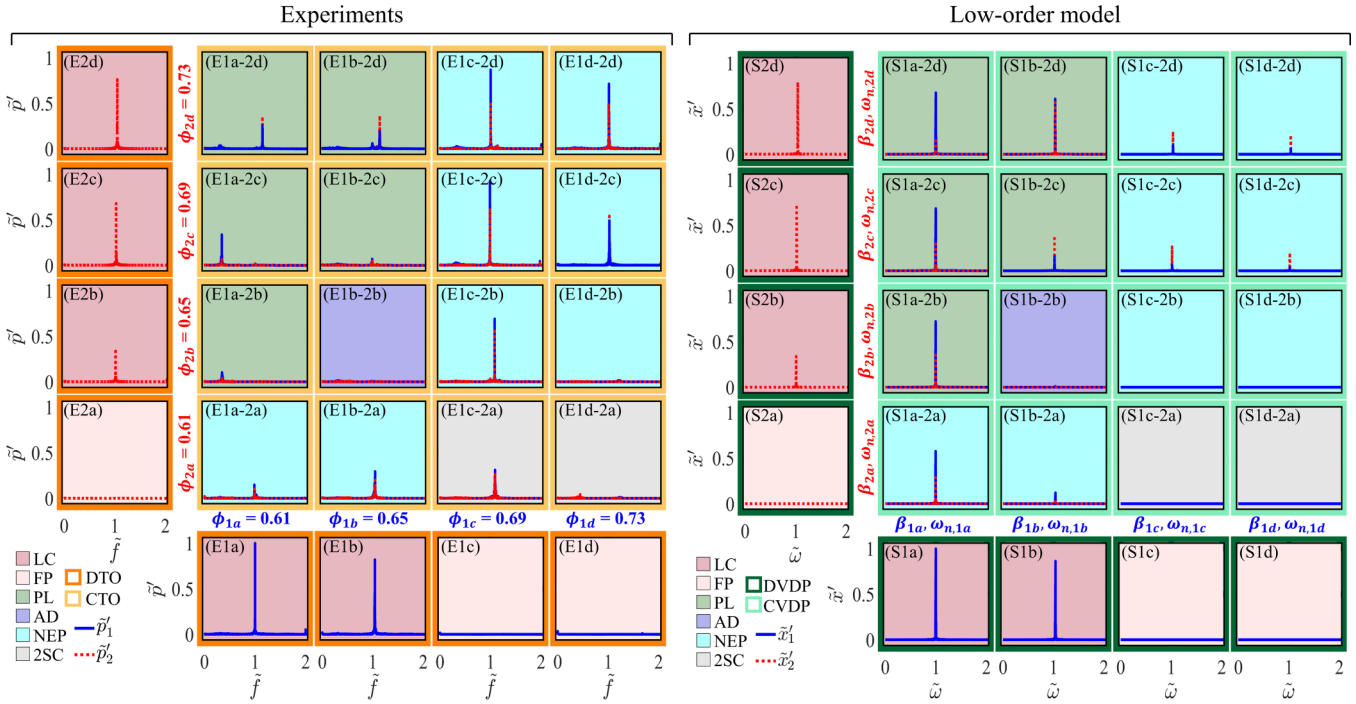

FIG. 4. Spectral comparison between thermoacoustic experiments (yellow borders) [34,35] and VDP simulations (green borders) under asymmetric inlet-length conditions ($l_{\text{inlet},1} = 340$ mm, $l_{\text{inlet},2} = 680$ mm). The decoupled thermoacoustic oscillators (DTO: no cross-talk tube) and decoupled VDP oscillators (DVDP: $k_d = k_\tau = 0$) are denoted by dark yellow and dark green borders, respectively. The coupled thermoacoustic oscillators (CTO: $\epsilon = 1.0$, $\eta = 0.25$) and coupled VDP oscillators (CVDP: $k_d = k_\tau = 0.013$, $\tau = 1.6$) are denoted by light yellow and light green borders, respectively. Experimental calibration of the VDP model gives $(\beta_{1a}, \beta_{1b}, \beta_{1c}, \beta_{1d}) = (0.04, 0.03, -0.01, -0.02)$, $(\beta_{2a}, \beta_{2b}, \beta_{2c}, \beta_{2d}) = (-0.005, 0.005, 0.025, 0.025)$, $(\omega_{n,1a}, \omega_{n,1b}, \omega_{n,1c}, \omega_{n,1d}) = (1.01, 1.05, 1.06, 1.07)$, and $(\omega_{n,2a}, \omega_{n,2b}, \omega_{n,2c}, \omega_{n,2d}) = (1.00, 1.02, 1.03, 1.05)$. Legend: LC = limit cycle; FP = fixed point; PL = phase locking; AD = amplitude death; NEP = nonlinear energy pumping; 2SC = two steady oscillators coupled together.

In addition to QP and PL, NEP can also be reproduced by the VDP model. This can be seen in the partially (Fig. 2: S1c–S2b, S1d–S2b) and completely (Fig. 2: S1c–S2a, S1d–S2a) suppressed states that arise when an initially steady oscillator (Fig. 2: S1c or S1d), representing an energy sink, is coupled to a limit-cycle oscillator (Fig. 2: S2a or S2b). We observe a similar suppression of the self-excited mode in the thermoacoustic system.

There are, however, two notable features of the thermoacoustic system that could not be reproduced by the VDP model: (i) the triggering of a nonlinearly unstable mode when a steady oscillator is coupled to a limit-cycle oscillator (Fig. 2: S1c–S2b $\nrightarrow$ E1c–E2b), and (ii) the generation of globally synchronized limit-cycle motion when two initially steady oscillators are coupled together (Fig. 2: S1c–S2c $\nrightarrow$ E1c–E2c).

B. Asymmetric inlet length: $l_{\text{inlet},2} = 2\,l_{\text{inlet},1}$

Next we consider experiments in which the two thermoacoustic oscillators have different inlet lengths: $l_{\text{inlet},1} = 340$ mm and $l_{\text{inlet},2} = 680$ mm [34,35]. We keep all the other operating and coupling conditions the same as they were in Sec. III A. Figure 4 shows the pressure spectra from the experiments, with the dark yellow borders corresponding to the decoupled cases (no cross-talk tube) and the light yellow borders corresponding to the coupled cases ($\epsilon = 1.0$, $\eta = 0.25$), as per Fig. 2. The case labels are also defined as per Fig. 2.

We find a variety of synchronization phenomena in Fig. 4. Some of these—such as PL, and NEP from a limit-cycle mode to an energy sink—were also seen in the symmetric inlet-length cases (Fig. 2). There are, however, subtle differences when the inlet lengths become asymmetric. For example, we find two unusual PL cases (Fig. 4: E1a–E2b, E1a–E2c) in which the global frequency of the synchronized system is markedly lower than the limit-cycle frequencies of the individual decoupled thermoacoustic oscillators. We attribute this low-frequency synchronization to the emergence of a new half-wave push-pull mode in the coupled thermoacoustic system [34]. This long-wavelength mode, however, is sufficiently damped when the inlet lengths are symmetric (Fig. 2).

We find unusual cases of NEP as well (Fig. 4: E1c–E2b, E1c–E2c, E1c–E2d): the amplitude of the periodic motion of the initially steady oscillator (blue peak) is even higher than that of the limit-cycle oscillator itself (red peak). This behavior could be due to the triggering of a nonlinearly unstable mode in the initially steady oscillator (Fig. 4: E1c), which was discussed earlier (Fig. 2: E1c). After being triggered, this new mode synchronizes with the natural limit-cycle mode from the other oscillator (Fig. 4: E2b, E2c, E2d), causing both oscillators to evolve at the same global frequency.

Crucially, we find a phenomenon not seen in the symmetric inlet-length cases of Fig. 2: AD (Fig. 4: E1b–E2b). As noted in Sec. I, AD refers to the quenching of an ensemble of self-

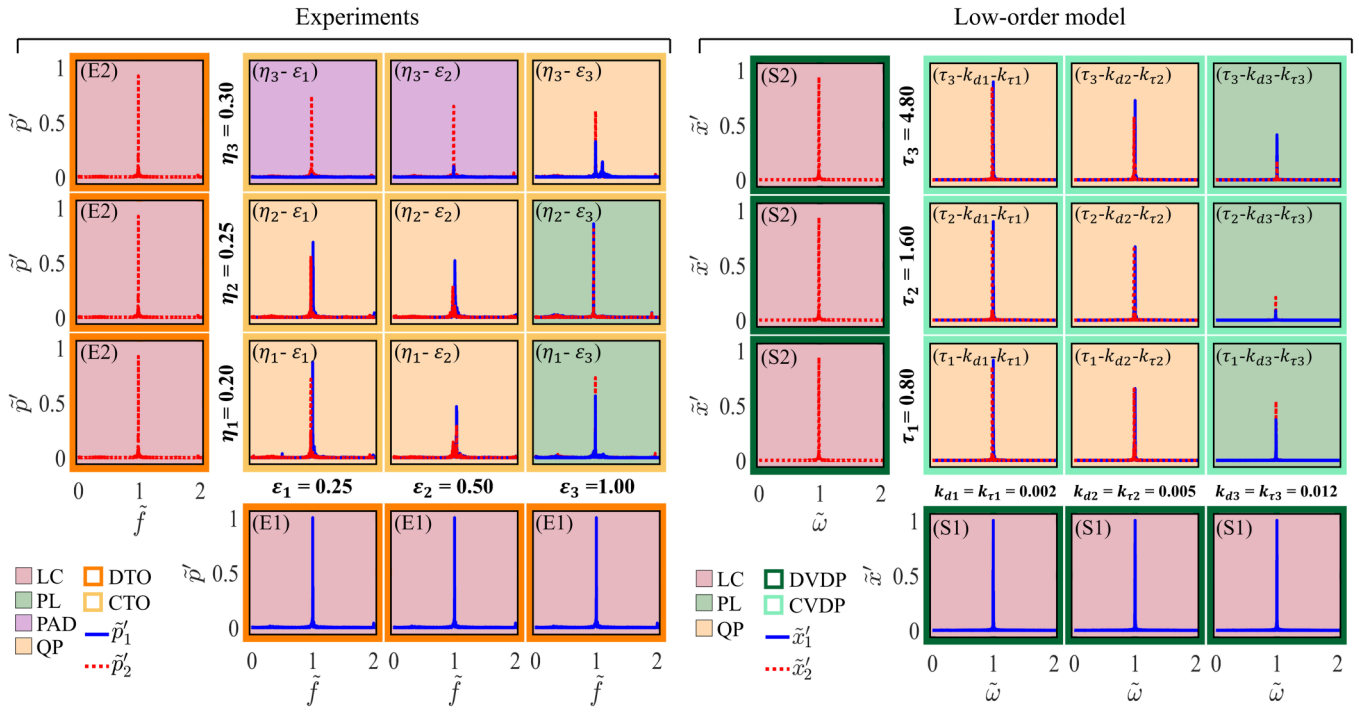

FIG. 5. Spectral comparison between thermoacoustic experiments (yellow borders) [35] and VDP simulations (green borders) under symmetric inlet-length conditions ($l_{\text{inlet},1} = l_{\text{inlet},2} = 340$ mm) and symmetric equivalence-ratio conditions [$(\phi_1, \phi_2) = (0.65, 0.65)$]. The decoupled thermoacoustic oscillators (DTO: no cross-talk tube) and decoupled VDP oscillators (DVDP: $k_d = k_\tau = 0$) are denoted by dark yellow and dark green borders, respectively. The coupled thermoacoustic oscillators (CTO) and coupled VDP oscillators (CVDP) are denoted by light yellow and light green borders, respectively. Experimental calibration of the VDP model gives $\beta_1 = 0.02$, $\beta_2 = 0.018$, $\omega_{n,1} = 1.00$, and $\omega_{n,2} = 0.98$. Legend: LC = limit cycle; PL = phase locking; QP = quasiperiodicity; PAD = partial amplitude death.

excited oscillators when they are coupled appropriately, leaving the overall coupled system in a steady state [20,21]. This phenomenon has been used to passively suppress self-excited oscillations in various systems, such as electronic circuits and lasers [20,21]. In fluid mechanics, AD has been observed experimentally in laminar thermoacoustic systems [22–25], but rarely in turbulent ones [34]. Although notable progress has been made to model the effects of dissipative and time-delay coupling on the onset of AD [22,23,32,62], the focus to date has been on laminar thermoacoustic systems. As we will show below, this study represents the first successful attempt to model AD in a turbulent thermoacoustic system.

As for the VDP model (Fig. 4: green borders), we find that it can reproduce many of the phenomena observed experimentally, such as synchronization leading to PL, NEP from a limit-cycle mode to an energy sink, and even AD. The value of $\tau = 1.6$ at which AD occurs is consistent with the time-delay criterion proposed theoretically by Reddy *et al.* [26] and Atay [28] and demonstrated experimentally by Reddy *et al.* [63] and Biwa *et al.* [22]: AD tends to occur when the time delay is near an odd integer multiple of a quarter period of the oscillations, i.e., $\tau = nT/4 = n\pi/2\omega$, where $\omega \approx 1$ here and n is odd. The fact that AD is observed at only one of the many combinations shown in Fig. 4 suggests that its emergence depends not just on the coupling parameters, but also on the parameters of the individual oscillators themselves, such as their relative amplitudes and frequencies.

However, despite the similarities between the simulations and experiments, there are several key differences. These include the inability of the VDP model to reproduce (i) the low frequency of synchronization observed during PL (Fig. 4: E1a–E2b, E1a–E2c), and (ii) the mode amplification in the initially steady oscillator observed during NEP (Fig. 4: E1c–E2b, E1c–E2c, E1c–E2d).

C. Dissipative and time-delay coupling

We now explore the effects of the coupling parameters. First we consider experiments in which the nondimensional diameter ($\epsilon \equiv D_{\text{XT}}/D_{\text{XT},0}$) and length ($\eta \equiv l_{\text{XT}}/l_c$) of the cross-talk tube are independently varied: $\epsilon = [0.25, 0.50, 1.00]$ and $\eta = [0.20, 0.25, 0.30]$. Here we keep the inlet lengths the same ($l_{\text{inlet},1} = l_{\text{inlet},2} = 340$ mm) but use two different sets of equivalence ratios: a symmetric set where $(\phi_1, \phi_2) = (0.65, 0.65)$ [Fig. 5], and an asymmetric set where $(\phi_1, \phi_2) = (0.69, 0.61)$ [Fig. 6].

Starting with the symmetric-ϕ cases, we find that, when decoupled, both thermoacoustic oscillators are individually self-excited at a limit cycle (Fig. 5: E1, E2). When coupled, they exhibit QP if both η and ϵ are small (Fig. 5: η_1–ϵ_1, η_1–ϵ_2, η_2–ϵ_1, η_2–ϵ_2). However, if either η or ϵ is large, PAD or PL occurs, respectively. When both η and ϵ are large (Fig. 5: η_3–ϵ_3), a new thermoacoustic mode emerges at a slightly higher frequency. This new mode interacts with the original limit-cycle mode, producing QP on a $\mathbb{T}^2$ torus attractor.

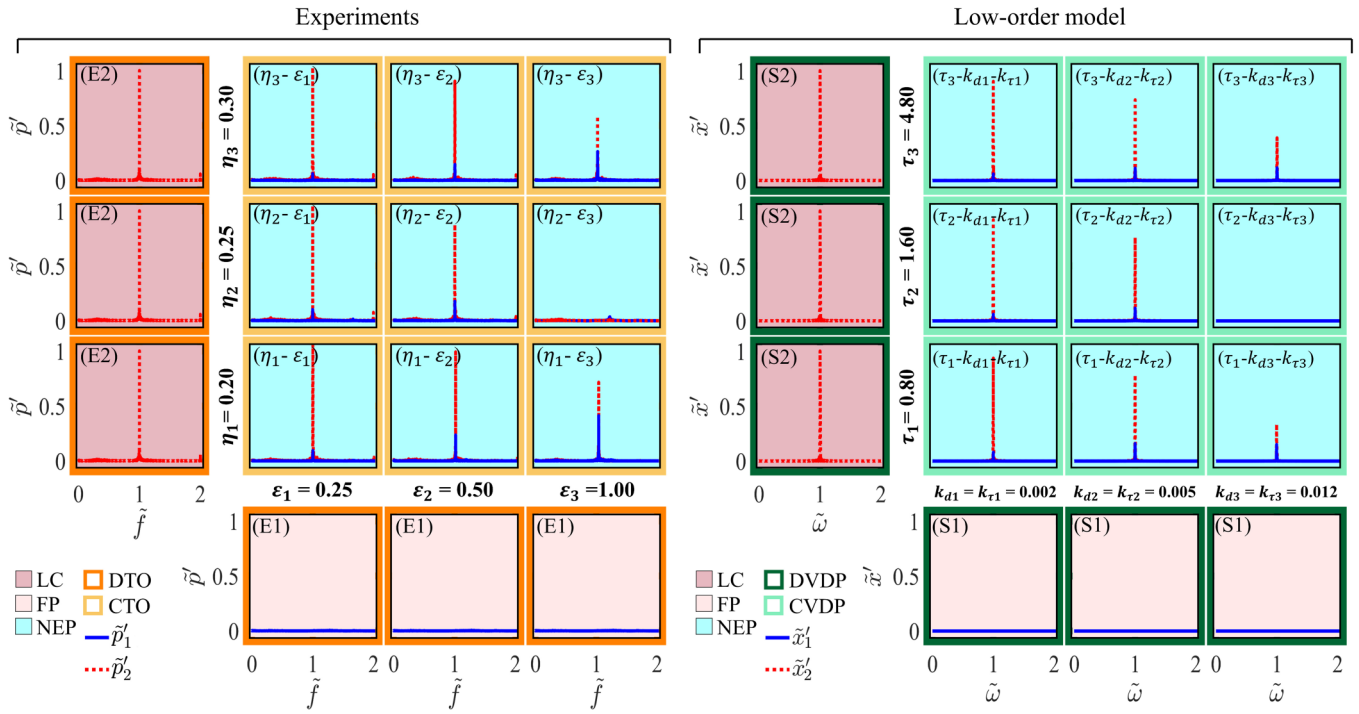

FIG. 6. The same as for Fig. 5 but under asymmetric equivalence-ratio conditions $[(\phi_1,\ \phi_2) = (0.69,\ 0.61)]$. Experimental calibration of the VDP model gives $\beta_1 = -0.015$, $\beta_2 = 0.025$, $\omega_{n,1} = 0.98$, and $\omega_{n,2} = 1.00$. The two VDP oscillators are coupled to each other using the same parameters ($k_d = k_\tau$, τ) as in Fig. 5. Legend: LC = limit cycle; FP = fixed point; NEP = nonlinear energy pumping.

As for the simulations, we find that the VDP model can reproduce all the synchronization phenomena observed experimentally, with the exception of PAD (Fig. 5: η_3–ϵ_1, η_3–ϵ_2) and the QP case found at the largest values of η and ϵ (Fig. 5: η_3–ϵ_3). Crucially, the four QP cases found at small and intermediate values of η and ϵ (Fig. 5: η_1–ϵ_1, η_1–ϵ_2, η_2–ϵ_1, η_2–ϵ_2) are reproduced well by the model with small and intermediate values of τ and $k_d = k_\tau$. In these QP cases, two incommensurate modes arise in both VDP oscillators, producing $\mathbb{T}^2$ dynamics similar to that seen in Figs. 3(a2)–3(c2). When k_d (and thus k_τ) increases, however, the two incommensurate modes synchronize to a common frequency (Fig. 5: τ_1–k_{d3}–$k_{\tau 3}$, τ_2–k_{d3}–$k_{\tau 3}$), producing a PL state similar to that observed experimentally (Fig. 5: η_1–ϵ_3, η_2–ϵ_3), albeit with reduced amplitudes. This PL state is similar to that seen in Figs. 3(d2)–3(f2). Although we do not observe PAD in the model, this is not a limitation of the model itself [28], but is due to the specific range of system and coupling parameters used here.

Turning to the asymmetric-ϕ cases, we find that, when decoupled, one thermoacoustic oscillator is initially steady (Fig. 6: E1), but the other is initially self-excited at a limit cycle (Fig. 6: E2). When coupled, they exhibit NEP for all the examined values of η and ϵ. These NEP cases include (i) a complete suppression of the limit-cycle mode, resulting in a steady coupled system (Fig. 6: η_2–ϵ_3), and (ii) mode amplification in the initially steady oscillator, resulting in the two oscillators evolving at a common frequency but with different amplitudes. The model can accurately reproduce these synchronization phenomena, including the case where a limit-cycle oscillator is completely quenched via coupling to a steady oscillator (Fig. 6: τ_2–k_{d3}–$k_{\tau 3}$). As well as reinforcing the analogy between $k_d = k_\tau$ and ϵ and between τ and η, these results show that the mutual synchronization of two turbulent thermoacoustic oscillators can be modeled with just a pair of VDP oscillators interacting via dissipative and time-delay coupling.

IV. CONCLUSIONS

We have used a low-order model to investigate the mutual synchronization of two thermoacoustic oscillators coupled via a cross-talk tube. Each oscillator consists of a lean-premixed CH_4-air flame stabilized in the turbulent swirling flow of a cylindrical combustor. The model consists of two VDP oscillators coupled via dissipative and time-delay terms. By varying the parameters of the model, we were able to show that it can reproduce many of the synchronization phenomena observed experimentally, such as amplitude death, desynchronization (quasiperiodicity), synchronization (phase locking), and nonlinear energy pumping from a limit-cycle mode to a damped mode, i.e., to an energy sink. However, we also found several phenomena that could not be reproduced by the model. These include (i) the triggering of a nonlinearly unstable mode when an initially steady oscillator is coupled to a limit-cycle oscillator, e.g., Fig. 2: E1c–E2b; (ii) the generation of globally synchronized limit-cycle motion when two initially steady oscillators are coupled together, e.g., Fig. 2: E1c–E2c; (iii) mode amplification in an initially steady oscillator during nonlinear energy pumping, e.g., Fig. 4: E1c–E2d; and (iv) partial amplitude death, e.g., Fig. 5(η_3–ϵ_1). The inability of the model to reproduce some of these phenomena, such as partial amplitude death, may be due to the specific values of the system and coupling parameters used in this study,

whereas others may be due to the simplicity of the model itself: (i) each VDP oscillator contains just a single self-excited or damped mode, whereas an actual thermoacoustic oscillator typically contains multiple such modes interacting with one another; and (ii) the VDP kernel used here contains up to only cubic nonlinearity and thus generates a supercritical Hopf bifurcation in the decoupled state, whereas the simplest oscillator model (normal form) exhibiting triggering of a nonlinearly unstable mode should have at least quintic nonlinearity. In this study, we did not explore higher-order nonlinearities because our aim was to keep the model as simple as possible. Nevertheless, despite its simplicity, the model was still able to reproduce many of the phenomena observed experimentally. Crucially, the fact that the mutual synchronization dynamics of a turbulent thermoacoustic system can be reproduced with just a low-order VDP model suggests that such a model could be used (i) to aid the analysis and interpretation of experimental data collected from real combustion systems, and (ii) to identify new strategies for quenching self-excited thermoacoustic oscillations, e.g., by exploiting universal phenomena such as nonlinear energy pumping and amplitude death. With further development (e.g., via asymptotic methods [58,59]), this modeling approach could provide a means of predicting the synchronization dynamics of practical thermoacoustic systems, such as gas turbines and rocket engines.

ACKNOWLEDGMENTS

Y.G. and L.K.B.L. were supported by the Research Grants Council of Hong Kong (Projects No. 16210418, No. 16210419, and No. 16235716) and the Guangdong–Hong Kong–Macao Joint Laboratory for Data-Driven Fluid Mechanics and Engineering Applications (Project No. 2020B1212030001). K.M. and K.T.K. were supported by a National Research Foundation of Korea (NRF) grant funded by the Korean government (MSIT) (Grant No. 2019R1A2C1003208).

[1] H. Gotoda, Y. Okuno, K. Hayashi, and S. Tachibana, Characterization of degeneration process in combustion instability based on dynamical systems theory, Phys. Rev. E **92**, 052906 (2015).

[2] S. Murayama and H. Gotoda, Attenuation behavior of thermoacoustic combustion instability analyzed by a complex-network and synchronization-based approach, Phys. Rev. E **99**, 052222 (2019).

[3] T. C. Lieuwen and V. Yang, *Combustion Instabilities in Gas Turbine Engines*, Progress in Astronautics and Aeronautics (AIAA, Reston, VA, 2005).

[4] A. P. Dowling, Nonlinear self-excited oscillations of a ducted flame, J. Fluid Mech. **346**, 271 (1997).

[5] Y. Huang and V. Yang, Dynamics and stability of lean-premixed swirl-stabilized combustion, Prog. Energ. Combust. **35**, 293 (2009).

[6] S. Candel, Combustion dynamics and control: Progress and challenges, P. Combust. Inst. **29**, 1 (2002).

[7] A. P. Dowling and A. S. Morgans, Feedback control of combustion oscillations, Annu. Rev. Fluid Mech. **37**, 151 (2005).

[8] H. Gotoda, Y. Shinoda, M. Kobayashi, Y. Okuno, and S. Tachibana, Detection and control of combustion instability based on the concept of dynamical system theory, Phys. Rev. E **89**, 022910 (2014).

[9] T. Poinsot, Prediction and control of combustion instabilities in real engines, P. Combust. Inst. **36**, 1 (2017).

[10] T. Kobayashi, S. Murayama, T. Hachijo, and H. Gotoda, Early Detection of Thermoacoustic Combustion Instability Using a Methodology Combining Complex Networks and Machine Learning, Phys. Rev. Appl. **11**, 064034 (2019).

[11] S. Luque, V. Kanjirakkad, I. Aslanidou, R. Lubbock, B. Rosic, and S. Uchida, A new experimental facility to investigate combustor–turbine interactions in gas turbines with multiple can combustors, J. Eng. Gas Turb. Power **137**, 051503 (2015).

[12] H. C. Mongia, T. J. Held, G. C. Hsiao, and R. P. Pandalai, Challenges and progress in controlling dynamics in gas turbine combustors, J. Propul. Power **19**, 822 (2003).

[13] P. Kaufmann, W. Krebs, R. Valdes, and U. Wever, 3D thermoacoustic properties of single can and multi can combustor configurations, in *Turbo Expo: Power for Land, Sea, and Air*, Vol. 43130 (American Society of Mechanical Engineers, New York, 2008), pp. 527–538.

[14] F. Farisco, L. Panek, and J. B. W. Kok, Thermo-acoustic cross-talk between cans in a can-annular combustor, Int. J. Spray Combust. **9**, 452 (2017).

[15] G. Ghirardo, C. Di Giovine, J. P. Moeck, and M. R. Bothien, Thermoacoustics of can-annular combustors, J. Eng. Gas Turb. Power **141**, 011007 (2019).

[16] G. Bonciolini and N. Noiray, Synchronization of thermoacoustic modes in sequential combustors, J. Eng. Gas Turb. Power **141**, 031010 (2019).

[17] R. I. Sujith and V. R. Unni, Complex system approach to investigate and mitigate thermoacoustic instability in turbulent combustors, Phys. Fluids **32**, 061401 (2020).

[18] R. I. Sujith and V. R. Unni, Dynamical systems and complex systems theory to study unsteady combustion, P. Combust. Inst. **38**, 3445 (2020).

[19] R. E. Mirollo and S. H. Strogatz, Amplitude death in an array of limit-cycle oscillators, J. Stat. Phys. **60**, 245 (1990).

[20] A. Pikovsky, M. Rosenblum, and J. Kurths, *Synchronization: A Universal Concept in Nonlinear Sciences* (Cambridge University Press, Cambridge, UK, 2003).

[21] A. Balanov, N. Janson, D. Postnov, and O. Sosnovtseva, *Synchronization: From Simple to Complex* (Springer Science & Business Media, Berlin, 2008).

[22] T. Biwa, S. Tozuka, and T. Yazaki, Amplitude Death in Coupled Thermoacoustic Oscillators, Phys. Rev. Appl. **3**, 034006 (2015).

[23] H. Hyodo and T. Biwa, Stabilization of thermoacoustic oscillators by delay coupling, Phys. Rev. E **98**, 052223 (2018).

[24] S. Dange, K. Manoj, S. Banerjee, S. A. Pawar, S. Mondal, and R. I. Sujith, Oscillation quenching and phase-flip bifurcation in coupled thermoacoustic systems, Chaos **29**, 093135 (2019).

[25] H. Hyodo, M. Iwasaki, and T. Biwa, Suppression of Rijke tube oscillations by delay coupling, J. Appl. Phys. **128**, 094902 (2020).

[26] D. V. Ramana Reddy, A. Sen, and G. L. Johnston, Time Delay Induced Death in Coupled Limit Cycle Oscillators, Phys. Rev. Lett. **80**, 5109 (1998).

[27] K. Konishi, Amplitude death induced by dynamic coupling, Phys. Rev. E **68**, 067202 (2003).

[28] F. M. Atay, Total and partial amplitude death in networks of diffusively coupled oscillators, Physica D **183**, 1 (2003).

[29] G. Saxena, A. Prasad, and R. Ramaswamy, Dynamical effects of integrative time-delay coupling, Phys. Rev. E **82**, 017201 (2010).

[30] G. Saxena, A. Prasad, and R. Ramaswamy, Amplitude death: The emergence of stationarity in coupled nonlinear systems, Phys. Rep. **521**, 205 (2012).

[31] D. G. Aronson, G. B. Ermentrout, and N. Kopell, Amplitude response of coupled oscillators, Physica D **41**, 403 (1990).

[32] N. Thomas, S. Mondal, S. A. Pawar, and R. I. Sujith, Effect of time-delay and dissipative coupling on amplitude death in coupled thermoacoustic oscillators, Chaos **28**, 033119 (2018).

[33] W. Liu, J. Xiao, and J. Yang, Partial amplitude death in coupled chaotic oscillators, Phys. Rev. E **72**, 057201 (2005).

[34] H. Jegal, K. Moon, J. Gu, L. K. B. Li, and K. T. Kim, Mutual synchronization of two lean-premixed gas turbine combustors: Phase locking and amplitude death, Combust. Flame **206**, 424 (2019).

[35] K. Moon, Y. Guan, L. K. B. Li, and K. T. Kim, Mutual synchronization of two flame-driven thermoacoustic oscillators: Dissipative and time-delayed coupling effects, Chaos **30**, 023110 (2020).

[36] M. L. Cartwright, Balthazar van der Pol, J. London Math. Soc. **35**, 367 (1960).

[37] L. K. B. Li and M. P. Juniper, Lock-in and quasiperiodicity in a forced hydrodynamically self-excited jet, J. Fluid Mech. **726**, 624 (2013).

[38] L. K. B. Li and M. P. Juniper, Lock-in and quasiperiodicity in hydrodynamically self-excited flames: Experiments and modelling, P. Combust. Inst. **34**, 947 (2013).

[39] Y. Guan, V. Gupta, K. Kashinath, and L. K. B. Li, Open-loop control of periodic thermoacoustic oscillations: Experiments and low-order modelling in a synchronization framework, P. Combust. Inst. **37**, 5315 (2019).

[40] M. Lee, Y. Zhu, L. K. B. Li, and V. Gupta, System identification of a low-density jet via its noise-induced dynamics, J. Fluid Mech. **862**, 200 (2019).

[41] M. Lee, Y. Guan, V. Gupta, and L. K. B. Li, Input-output system identification of a thermoacoustic oscillator near a Hopf bifurcation using only fixed-point data, Phys. Rev. E **101**, 013102 (2020).

[42] M. Lee, K. T. Kim, V. Gupta, and L. K. B. Li, System identification and early warning detection of thermoacoustic oscillations in a turbulent combustor using its noise-induced dynamics, Proc. Combust. Inst. **38**, 6025 (2021).

[43] F. Takens, Detecting strange attractors in turbulence, in *Dynamical Systems and Turbulence*, Lecture Notes in Mathematics, edited by D. A. Rand and L. S. Young (Springer-Verlag, New York, 1981), pp. 366–381.

[44] P. Grassberger and I. Procaccia, Characterization of Strange Attractors, Phys. Rev. Lett. **50**, 346 (1983).

[45] R. C. Hilborn, *Chaos and Nonlinear Dynamics: An Introduction for Scientists and Engineers* (Oxford University Press, Oxford, UK, 2000).

[46] L. Kabiraj, A. Saurabh, N. Karimi, A. Sailor, E. Mastorakos, A. P. Dowling, and C. O. Paschereit, Chaos in an imperfectly premixed model combustor, Chaos **25**, 023101 (2015).

[47] Y. Guan, L. K. B. Li, B. Ahn, and K. T. Kim, Chaos, synchronization, and desynchronization in a liquid-fueled diffusion-flame combustor with an intrinsic hydrodynamic mode, Chaos **29**, 053124 (2019).

[48] B. Boashash, Estimating and interpreting the instantaneous frequency of a signal. II. Algorithms and applications, Proc. IEEE **80**, 540 (1992).

[49] Y. Guan, V. Gupta, M. Wan, and L. K. B. Li, Forced synchronization of quasiperiodic oscillations in a thermoacoustic system, J. Fluid Mech. **879**, 390 (2019).

[50] L. K. B. Li and M. P. Juniper, Phase trapping and slipping in a forced hydrodynamically self-excited jet, J. Fluid Mech. **735**, R5 (2013).

[51] S. Balusamy, L. K. B. Li, Z. Han, M. P. Juniper, and S. Hochgreb, Nonlinear dynamics of a self-excited thermoacoustic system subjected to acoustic forcing, P. Combust. Inst. **35**, 3229 (2015).

[52] K. Kashinath, L. K. B. Li, and M. P. Juniper, Forced synchronization of periodic and aperiodic thermoacoustic oscillations: Lock-in, bifurcations, and open-loop control, J. Fluid Mech. **838**, 690 (2018).

[53] K. T. Kim and S. Hochgreb, Measurements of triggering and transient growth in a model lean-premixed gas turbine combustor, Combust. Flame **159**, 1215 (2012).

[54] Y. Guan, W. He, M. Murugesan, Q. Li, P. Liu, and L. K. B. Li, Control of self-excited thermoacoustic oscillations using transient forcing, hysteresis and mode switching, Combust. Flame **202**, 262 (2019).

[55] K. Moon, H. Jegal, J. Gu, and K. T. Kim, Combustion-acoustic interactions through cross-talk area between adjacent model gas turbine combustors, Combust. Flame **202**, 405 (2019).

[56] O. Gendelman, L. I. Manevitch, A. F. Vakakis, and R. M'closkey, Energy pumping in nonlinear mechanical oscillators: Part I: Dynamics of the underlying Hamiltonian systems, ASME J. Appl. Mech. **68**, 34 (2001).

[57] G. Kerschen, Y. S. Lee, A. F. Vakakis, D. M. McFarland, and L. A. Bergman, Irreversible passive energy transfer in coupled oscillators with essential nonlinearity, SIAM J. Appl. Math. **66**, 648 (2005).

[58] O. V. Gendelman and T. Bar, Bifurcations of self-excitation regimes in a Van der Pol oscillator with a nonlinear energy sink, Physica D **239**, 220 (2010).

[59] Y. S. Lee, A. F. Vakakis, L. A. Bergman, and D. M. McFarland, Suppression of limit cycle oscillations in the van der Pol oscillator by means of passive nonlinear energy sinks, Struct. Control Health Monit. **13**, 41 (2006).

[60] Y. S. Lee, A. F. Vakakis, L. A. Bergman, D. M. McFarland, and G. Kerschen, Suppression aeroelastic instability using broadband passive targeted energy transfers, Part 1: Theory, AIAA J. **45**, 693 (2007).

[61] E. Gourdon and C. Lamarque, Energy pumping with various nonlinear structures: Numerical evidences, Nonlin. Dyn. **40**, 281 (2005).

[62] N. Thomas, S. Mondal, S. A. Pawar, and R. I. Sujith, Effect of noise amplification during the transition to amplitude death in coupled thermoacoustic oscillators, Chaos **28**, 093116 (2018).

[63] D. V. Ramana Reddy, A. Sen, and G. L. Johnston, Experimental Evidence of Time-Delay-Induced Death in Coupled Limit-Cycle Oscillators, Phys. Rev. Lett. **85**, 3381 (2000).